

TNI	Kozmická technika Príručka pre tepelnotechnický návrh Časť 6: Tepelné riadenie povrchov	TNI CEN/CLC/TR 17603-31-06 31 0540
------------	--	--

Space Engineering - Thermal design handbook - Part 6: Thermal Control Surfaces

Táto technická normalizačná informácia obsahuje anglickú verziu CEN/CLC/TR 17603-31-06:2021.
This Technical standard information includes the English version of CEN/CLC/TR 17603-31-06:2021.

Táto technická normalizačná informácia bola oznámená vo Vestníku ÚNMS SR č. 12/21

TECHNICAL REPORT
RAPPORT TECHNIQUE
TECHNISCHER BERICHT

**CEN/CLC/TR 17603-31-
06**

August 2021

ICS 49.140

English version

**Space Engineering - Thermal design handbook - Part 6:
Thermal Control Surfaces**

Ingénierie spatiale - Manuel de conception thermique -
Partie 6: Revêtements de Contrôle Thermique

Raumfahrttechnik - Handbuch für thermisches Design -
Teil 6: Oberflächen zur Thermalkontrolle

This Technical Report was approved by CEN on 21 June 2021. It has been drawn up by the Technical Committee CEN/CLC/JTC 5.

CEN and CENELEC members are the national standards bodies and national electrotechnical committees of Austria, Belgium, Bulgaria, Croatia, Cyprus, Czech Republic, Denmark, Estonia, Finland, France, Germany, Greece, Hungary, Iceland, Ireland, Italy, Latvia, Lithuania, Luxembourg, Malta, Netherlands, Norway, Poland, Portugal, Republic of North Macedonia, Romania, Serbia, Slovakia, Slovenia, Spain, Sweden, Switzerland, Turkey and United Kingdom.



**CEN-CENELEC Management Centre:
Rue de la Science 23, B-1040 Brussels**

Table of contents

European Foreword.....	14
1 Scope.....	15
2 References	16
3 Terms, definitions and symbols	17
3.1 Terms and definitions	17
3.2 Abbreviated terms.....	17
3.3 Symbols.....	18
4 General introduction	21
5 Coatings	23
5.1 General.....	23
5.2 Solar reflectors	25
5.2.1 Titanium Dioxide-Polymethyl Vinyl Siloxane.....	25
5.2.2 Zinc Oxide-Potassium Silicate.....	32
5.2.3 Zinc Orthotitanate-Potassium Silicate	52
5.2.4 Zinc Oxide-Methylsilicone	136
5.2.5 Zinc Oxide-Potassium Silicate.....	163
5.2.6 Silver vacuum deposited on fused Silica	196
5.2.7 Silver vacuum deposited on fused Silica with a conductive coating.....	251
5.3 Total reflectors.....	274
5.3.1 Leafing Aluminium-Silicone	274
5.4 Total absorbers.....	279
5.4.1 Carbon black-Acrylic resin.....	279
6 Adhesive tapes	283
6.1 General.....	283
6.1.2 Adhesive properties	283
6.1.3 Curing of adhesive tapes.....	285
6.1.4 General purpose adhesive tapes.....	286
6.2 Application and handling.....	298
6.2.1 Application	298

CEN/CLC/TR 17603-31-06:2021 (E)

6.2.2	Cleaning.....	298
6.2.3	Handling.....	299
6.2.4	Repairing	300
6.3	Degradation	300
6.3.1	Introduction	300
6.3.2	Terrestrial degradation	300
6.3.3	Space degradation	300
6.3.4	Blistering	304
6.4	Relevant properties of thermal control tapes.....	307
6.5	Past spatial use	331
Bibliography.....		333

Figures

Figure 4-1: Basic types of thermal control coatings. T_R [K] is the equilibrium temperature of a coated isothermal sphere at 1 AU. From Touloukian, DeWitt & Hernicz (1972) [126].	21
Figure 4-2: Range of solar absorptance, α_s , and hemispherical total emittance, ε , covered by available thermal control coatings. From Touloukian, DeWitt & Hernicz (1972) [126].	22
Figure 5-1: UV radiation effects on solar absorptance, α_s , of Thermatrol 2A-100 vs. exposure time, t . From Breuch (1967) [22].	28
Figure 5-2: Change in solar absorptance, $\Delta\alpha_s$, of Thermatrol 2A-100, under various radiation conditions, vs. exposure time, t . From McCargo et al. (1971) [82].	28
Figure 5-3: Normal-hemispherical spectral reflectance, ρ_λ' , of Thermatrol 2A-100, measured by two different methods, vs. wavelength, λ . From Cunningham, Grammer & Smith (1969) [33].	29
Figure 5-4: Effect of Ultra-Violet Radiation on spectral reflectance, ρ_λ' , of Thermatrol 2A-100 vs. wavelength, λ . Most of the data, concerning bidirectional reflectance, are from Rittenhouse & Singletary (1969) [105], while dashed line and dotted line, normal-hemispherical reflectance, are from Cunningham, Grammer & Smith (1969) [33].	30
Figure 5-5: Variation of solar absorptance, α_s , with thickness, t_c . From Stevens (1971) [120].	36
Figure 5-6: Estimated changes in the solar absorptance, α_s , of Z-93 during the total mission profile for a near-Earth orbit. From McCargo, Spradley, Greenberg & McDonald (1971) [82].	45
Figure 5-7: Normal-hemispherical spectral reflectance, ρ_λ' , of Z-93 vs. wavelength, λ . All data are from Touloukian, DeWitt & Hernicz (1972) [126] except solid and dashed lines which are from Cunningham, Grammer & Smith (1969) [33].	47
Figure 5-8: Effect of Ultra-Violet Radiation on normal-hemispherical spectral reflectance, ρ_λ' , of Z-93 vs. wavelength, λ . Data points are from Touloukian,	

CEN/CLC/TR 17603-31-06:2021 (E)

DeWitt & Hernicz (1972) [126], while smooth curves are from Cunningham, Grammer & Smith (1969) [33].	49
Figure 5-9: Effect of Proton Radiation on normal-hemispherical spectral reflectance, ρ_{λ}' , of Z-93 vs. wavelength, λ . From Touloukian, DeWitt & Hernicz (1972) [126].	50
Figure 5-10: Hemispherical total emittance, ε , of Zinc Orthotitanate-Potassium Silicate Coatings vs. temperature, T . ○: SSR pigment, > phosphated. From Keyte (1975) [70]. ●: MOX pigment, > YB-71. From Harada & Wilkes (1979) [58]. □: YB-71. > AESC. From Ahern & Karperos (1983) [4].	60
Figure 5-11: Solar absorptance, α_s , of YB-71 vs. thickness, t_c . ○: From Harada & Wilkes (1979) [58]. ■: From measurements on 16 panels by AESC. Scatter is due to t_c variation. From Ahern & Karperos (1983) [4].	60
Figure 5-12: Solar absorptance, α_s , of Zinc Orthotitanate-Potassium Silicate coating vs. incidence angle, β . SSR pigment, phosphated. From Keyte (1975) [70].	63
Figure 5-13: Solar absorptance, α_s , of several YB-71 coatings vs. exposure time, t , as deduced from data of various spacecraft in geosynchronous orbits. Numbers corresponds to sample designations.	74
Figure 5-14: Normal-hemispherical spectral reflectance, ρ_{λ}' , of Zinc Orthotitanate-Potassium Silicate coatings vs. wavelength, λ .	76
Figure 5-15: Effect of Ultra-Violet Radiation on normal-hemispherical spectral reflectance, ρ_{λ}' , of Zinc Orthotitanate- Potassium Silicate coatings vs. wavelength, λ .	78
Figure 5-16: Effect of Protons Radiation on normal-hemispherical spectral reflectance, ρ_{λ}' , of Zinc Orthotitanate-Potassium Silicate coatings vs. wavelength, λ . From Gilligan & Zerlaut (1971) [46].	79
Figure 5-17: Hemispherical total emittance, ε , of S-13 G coating vs. temperature, T . 2×10^{-4} m thick coating on molybdenum substrate. From Spisz & Jack (1971) [119].	85
Figure 5-18: Hemispherical total emittance, ε , of S-13 and S-13 G coatings vs. exposure time, t , at 1-Sun level and 395 K. From Cunningham, Grammer & Smith (1969) [33]. Equal symbols correspond to the same sample. ○: > Sample 27; ●: > Sample 43; □: > Sample 28; ■: > Sample 44.	87
Figure 5-19: Variation of solar absorptance, α_s , of S-13 coating with coating thickness, t_c . ○: > Nominal composition. Sprayed on primed surface. Air dried. $T = 298$ K. (Designation in the ref.: 119 to 127). □: > ZnO in silicone binder. $T = 298$ K. (Designation in the ref.: 29, 30). From Touloukian, DeWitt & Hernicz (1972) [126].	89
Figure 5-20: Solar absorptance, α_s , of S-13 G coating vs. incidence angle, β . From Keyte (1975) [70].	90
Figure 5-21: Change in solar absorptance, $\Delta\alpha_s$, of S-13 and S-13 G coatings due to Protons and Alpha Particles Radiation vs. integrated flux, n .	94
Figure 5-22: Change in solar absorptance, $\Delta\alpha_s$, of S-13 G coating due to Electrons Radiation vs. integrated flux, n . Data taken in situ. Compiled by Bourrieau, Paillous & Romer (1976) [21].	96
Figure 5-23: Changes in solar absorptance of S-13 and S-13 G coatings. OSO III experiment. From Millard (1969) [84].	98





CEN/CLC/TR 17603-31-06:2021 (E)

Figure 5-24: Change in solar absorptance, $\Delta\alpha_s$, of S-13 coatings vs. flight time in ESH as measured in orbital flight. Prepared by the compiler after Touloukian, DeWitt & Hernicz (1972) [126].	99
Figure 5-25: Change in solar absorptance, $\Delta\alpha_s$, of S-13 G coating vs. flight time in ESH as measured in orbital flight. Prepared by the compiler after Touloukian, DeWitt & Hernicz (1972) [126].	100
Figure 5-26: Position on the sample holder of the samples 1 and 2, for irradiation and measurement. From Paillous (1976) [96].	104
Figure 5-27: Solar absorptance, α_s , of S-13 G/LO coating vs. flight time,	105
Figure 5-28: Variation of absorptance to emittance ratio, α/ε , of S-13 coating vs. flight time. Prepared by the compiler after Touloukian, DeWitt & Hernicz (1972) and Triolo (1973) [126].	106
Figure 5-29: Variation of absorptance to emittance ratio, α/ε , of S-13 G coating vs. flight time. Prepared by the compiler after Touloukian, DeWitt & Hernicz (1972) [126].	107
Figure 5-30: Normal-hemispherical spectral reflectance, ρ'_{λ} , of S-13 coating vs. wavelength, λ , for five different values of P-VC. G.E. LTV-602 binder. From Touloukian, DeWitt & Hernicz (1972) [126].	108
Figure 5-31: Effect of Ultra-violet Radiation on normal-hemispherical spectral reflectance, ρ'_{λ} , of S-13 coating vs. wavelength, λ . LTV-602 silicone binder. Two different pigment-binder ratios (PBR). From Touloukian, DeWitt & Hernicz (1972) [126].	109
Figure 5-32: Effect of Ultra-Violet Radiation on normal-hemispherical spectral reflectance, ρ'_{λ} , of S-13 coating vs. wavelength, λ . Several binders and PBRs. From Touloukian, DeWitt & Hernicz (1972) [126].	110
Figure 5-33: Effect of Ultra-Violet Radiation on normal-hemispherical spectral reflectance, ρ'_{λ} , of S-13 coating vs. wavelength, λ . From Touloukian, DeWitt & Hernicz (1972) [126].	111
Figure 5-34: Effect of Ultra-Violet Radiation on normal-hemispherical spectral reflectance, ρ'_{λ} , of S-13 coating vs. wavelength, λ . From Zerlaut, Rogers & Noble (1969) [144]. Drawn from Touloukian, DeWitt & Hernicz (1972) [126].	112
Figure 5-35: Effect of Ultra-Violet Radiation on normal-hemispherical spectral reflectance, ρ'_{λ} , of S-13 G coating vs. wavelength, λ . Two different pigment treatment processes. From Zerlaut, Rogers & Noble (1969) [144]. Drawn from Touloukian, DeWitt & Hernicz (1972) [126].	113
Figure 5-36: Effect of Ultra-Violet Radiation on normal-hemispherical spectral reflectance, ρ'_{λ} , of S-13 G coating vs. wavelength, λ . Sweated pigment. Two different solvent systems. From Zerlaut, Rogers & Noble (1969) [144]. Drawn from Touloukian, DeWitt & Hernicz (1972) [126].	114
Figure 5-37: Effect of Ultra-Violet Radiation on normal-hemispherical spectral reflectance, ρ'_{λ} , of S-13 G coating vs. wavelength, λ . Two different pigment treatment processes. Owens-Illinois 650 binder. From Zerlaut, Rogers & Noble (1969) [144]. Drawn from Touloukian, DeWitt & Hernicz (1972) [126].	115
Figure 5-38: Effect of Ultra-Violet Radiation on normal-hemispherical spectral reflectance, ρ'_{λ} , of S-13 G coating vs. wavelength, λ . Pigment was sifted prior to wet grinding. Paint grind time 3 h. From Zerlaut, Rogers & Noble (1969) [144]. Drawn from Touloukian, DeWitt & Hernicz (1972) [126].	116



CEN/CLC/TR 17603-31-06:2021 (E)

Figure 5-39: Effect of Ultra-Violet Radiation on normal-hemispherical spectral reflectance, ρ'_{λ} , of S-13 G coating vs. wavelength, λ . Silicated pigment with five mechanical perturbations. From Zerlaut, Rogers & Noble (1969) [144]. Drawn from Touloukian, DeWitt & Hernicz (1972) [126].	117
Figure 5-40: Effect of Ultra-Violet Radiation on normal-hemispherical spectral reflectance, ρ'_{λ} , of S-13 G coating vs. wavelength, λ . Plasma annealed and potassium silicate treated pigment. From Gilligan & Zerlaut (1971) [46].	118
Figure 5-41: Protons exposure effects on normal-hemispherical spectral reflectance, ρ'_{λ} , of S-13 coating vs. wavelength, λ . LTV-602 silicone binder. From Gillette, Brown, Seiler & Sheldon (1966) [54]. Drawn from Touloukian, DeWitt & Hernicz (1972) [126].	120
Figure 5-42: Protons exposure effects on normal-hemispherical spectral reflectance, ρ'_{λ} , of S-13 G coating vs. wavelength, λ . Plasma annealed and potassium silicate treated pigment. From Gilligan & Zerlaut (1971) [46].	121
Figure 5-43: Electrons exposure effects on normal-hemispherical spectral reflectance, ρ'_{λ} , of S-13 G coating vs. wavelength, λ . Radiation intensity 20 keV. Recovery after exposure. From Fogdall, Cannaday & Brown (1970) [43]. Drawn from Touloukian, DeWitt & Hernicz (1972) [126].	122
Figure 5-44: Electrons exposure effects on normal-hemispherical spectral reflectance, ρ'_{λ} , of S-13 G coating vs. wavelength, λ . Radiation intensity 80 keV. Recovery after exposure. From Fogdall, Cannaday & Brown (1970) [43]. Drawn from Touloukian, DeWitt & Hernicz (1972) [126].	124
Figure 5-45: Electrons exposure effects on normal-hemispherical spectral reflectance, ρ'_{λ} , of GSFC, 101-7 coating vs. wavelength, λ . Radiation intensity 20 keV. Different integrated fluxes. 101-7 is a coating, similar to S-13 G, developed by NASA Goddard. From Fogdall, Cannaday Brown (1970) [43]. Drawn from Touloukian, DeWitt & Hernicz (1972) [126].	125
Figure 5-46: Electrons exposure effects on normal-hemispherical spectral reflectance, ρ'_{λ} , of GSFC, 101-7 coating vs. wavelength, λ . Radiation intensity 80 keV. Different integrated fluxes. 101-7 is a coating, similar to S-13 G, developed by NASA Goddard. From Fogdall, Cannaday & Brown (1970) [43]. Drawn from Touloukian, DeWitt & Hernicz (1972) [126].	126
Figure 5-47: Electrons exposure effects on normal-hemispherical spectral reflectance, ρ'_{λ} , of GSFC, 101-7 coating vs. wavelength, λ . Radiation intensity 20 keV. Recovery after exposure. 101-7 is a coating, similar to S-13 G, developed by NASA Goddard. From Fogdall, Cannaday & Brown (1970) [43]. Drawn from Touloukian, DeWitt & Hernicz (1972) [126].	127
Figure 5-48: Electrons exposure effects on normal-hemispherical spectral reflectance, ρ'_{λ} , of GSFC, 101-7 coating vs. wavelength, λ . Radiation intensity 80 keV. Recovery after exposure. 101-7 is a coating, similar to S-13 G, developed by NASA Goddard. From Fogdall, Cannaday Brown (1970) [43]. Drawn from Touloukian, DeWitt & Hernicz (1972) [126].	128
Figure 5-49: Effect of Combined Exposure on normal-hemispherical spectral reflectance, ρ'_{λ} , of S-13 G coating vs. wavelength, λ . Plasma annealed and potassium silicate treated pigment. From Gilligan & Zerlaut (1971) [46].	130
Figure 5-50: Effect of Combined Exposure, simulating up to three years in geosynchronous orbit, on normal-hemispherical spectral reflectance, ρ'_{λ} , of S-13 G/LO coating vs. wavelength, λ . From Paillous (1976) [96].	131





CEN/CLC/TR 17603-31-06:2021 (E)

Figure 5-51: Effect of O ₂ bleaching, after Combined Exposure, on normal-hemispherical spectral reflectance, ρ'_{λ} , of S-13 G/LO coating vs. wavelength, λ . Curves of  and  are those shown in Figure 5-19. From Paillous (1976) [96].	132
Figure 5-52: Effect of Combined Exposure, simulating up to three years in geosynchronous orbit, on normal- hemispherical spectral reflectance, ρ'_{λ} , of S-13 G/LO coating vs. wavelength, λ . Curves of  and  are those shown in Figure 5-50. From Paillous (1976) [96].	133
Figure 5-53: Change in normal-hemispherical spectral absorptance, $\Delta\alpha'_{\lambda}$, of PSG 120 coating, due to Ultra-Violet Radiation, vs. exposure time, t . Wavelength, $\lambda = 0,46 \times 10^{-6}$ m. From Simon (1974) [118].	140
Figure 5-54: Change in normal-hemispherical spectral absorptance, $\Delta\alpha'_{\lambda}$, of PSG 120 coating, due to Ultra-Violet Radiation, vs. exposure time, t . Wavelength, $\lambda = 2,5 \times 10^{-6}$ m. Shaded zone in <i>a</i> is enlarged in <i>b</i> . See Explanation in the caption of Figure 5-53. From Simon (1974) [118].	141
Figure 5-55: Change in solar absorptance, $\Delta\alpha_s$, of PSG 120 coating, due to UV radiation, vs. exposure time, t . Shaded zone in <i>a</i> is enlarged in <i>b</i> . From Simon (1974) [118].	142
Figure 5-56: Estimated change in solar absorptance, α_s , of PSG 120 vs. time, t . From Paillous (1976) [96]. O: From Guillaumon & Guillin (1981) [52].	148
Figure 5-57: Bidirectional total radiation intensity of reflected flux, I'' , vs. cone angle, β' , for several values of the cone angle of the incident flux, β . PSG 120 coating. Incident and reflected fluxes are coplanar. I'' is measured by the response of a photocell attached to a photogoniometer. From ASTRAL (1976)a [6].	148
Figure 5-58: Effect of Ultra-Violet Radiation on normal-hemispherical spectral reflectance, ρ'_{λ} , of PSG 120 coating vs. wavelength, λ . Thick line: Before irradiation. $p < 1,3 \times 10^{-5}$ Pa. $T = 348$ K. Thin line: After irradiation. $p < 1,3 \times 10^{-5}$ Pa. $T = 348$ K. A Sun level. $t = 212$ ESH. From Simon (1973) [117].	149
Figure 5-59: Effect of Protons radiation on normal-hemispherical spectral reflectance, ρ'_{λ} , of PSG 120 coating vs. wavelength, λ . Radiation intensity $\cong 45$ keV. See Explanation in the caption of Figure 5-61. From Paillous, Amat, Marco & Panabiere (1977) [97].	150
Figure 5-60: Effect of Protons radiation on normal-hemispherical spectral reflectance, ρ'_{λ} , of PSG 120 coating vs. wavelength, λ . Radiation intensity $\cong 75$ keV. See Explanation in the caption of Figure 5-61. From Paillous, Amat, Marco & Panabiere (1977) [97].	151
Figure 5-61: Effect of Protons radiation on normal-hemispherical spectral reflectance, ρ'_{λ} , of PSG 120 coating vs. wavelength, λ . Radiation intensity $\cong 150$ keV. From Paillous, Amat, Marco & Panabiere (1977) [97].	151
Figure 5-62: Effect of Electrons Radiation on normal-hemispherical spectral reflectance, ρ'_{λ} , of PSG 120 coating vs. wavelength, λ . Radiation intensity $\cong 40$ keV. See Explanation in the caption of Figure 5-63. From Paillous, Amat, Marco & Panabiere (1977) [97].	153
Figure 5-63: Effect of Electrons Radiation on normal-hemispherical spectral reflectance, ρ'_{λ} , of PSG 120 coating vs. wavelength, λ . Radiation intensity $\cong 80$ keV. From Paillous, Amat, Marco & Panabiere (1977) [97].	153

CEN/CLC/TR 17603-31-06:2021 (E)

Figure 5-64: Effect of Electrons Radiation on normal-hemispherical spectral reflectance, ρ'_{λ} , of PSG 120 coating vs. wavelength, λ . Radiation intensity \cong 210 keV. From Paillous, Amat, Marco & Panabiere (1977) [97].	154
Figure 5-65: Change in normal-hemispherical spectral reflectance, ρ'_{λ} , of PSG 120 coating, due to particulate irradiation, vs. penetration range, X_d . Wavelength, $\lambda = 2,05 \times 10^{-6}$ m. From Bourrieau (1978) [19].	157
Figure 5-66: Effect of Combined Exposure, simulating up to three years in geosynchronous orbit, on normal-hemispherical spectral reflectance, ρ'_{λ} , of PSG 120 coating vs. wavelength, λ . From Paillous (1976) [96].	157
Figure 5-67: Effect of O ₂ bleaching, after Combined Exposure, on normal-hemispherical spectral reflectance, ρ'_{λ} , of PSG 120 coating vs. wavelength, λ . Curves  and  are those shown in Figure 5-66. From Paillous (1976) [96].	158
Figure 5-68: Change in normal-hemispherical spectral absorptance, $\Delta\alpha'_{\lambda}$, of PSZ 184 coating, due to UV Radiation, vs. exposure time, t . Wavelength, $\lambda = 0,46 \times 10^{-6}$ m. See Explanation in the caption of Figure 5-69. From Simon (1974) [118].	166
Figure 5-69: Change in normal-hemispherical spectral absorptance, $\Delta\alpha'_{\lambda}$, of PSZ 184 coating, due to UV Radiation, vs. exposure time, t . Wavelength, $\lambda = 2,5 \times 10^{-6}$ m. From Simon (1974) [118].	167
Figure 5-70: Change in solar absorptance, $\Delta\alpha_s$, of PSZ 184 coating, due to UV Radiation, vs. exposure time, t . Shaded zone in <i>a</i> is enlarged in <i>b</i> . From Simon (1974) [118].	168
Figure 5-71: Estimated change in solar absorptance, α_s , of PSZ 184 vs. time, t . From Paillous (1976) [96].	173
Figure 5-72: Effect of Ultra-Violet Radiation on normal-hemispherical spectral reflectance, ρ'_{λ} , of PSZ 184 coating vs. wavelength, λ . Thick line: Before irradiation. $p < 1,3 \times 10^{-5}$ Pa. Thin line: After irradiation. $p < 1,3 \times 10^{-5}$ Pa. 1 Sun level. Neither sample temperature nor exposure time are given. From Simon (1974) [118].	174
Figure 5-73: Effect of Protons Radiation on normal-hemispherical spectral reflectance, ρ'_{λ} , of PSZ 184 coating vs. wavelength, λ . <i>a</i> Coating on P 131 primer. <i>b</i> Coating on silicated primer. Radiation intensity \cong 45 keV. See Explanation in the caption of Figure 5-74. From Paillous, Amat, Marco & Panabiere (1977) [97].	175
Figure 5-74: Effect of Protons Radiation on normal-hemispherical spectral reflectance, ρ'_{λ} , of PSZ 184 coating, on silicated primer, vs. wavelength, λ . Radiation intensity \cong 75 keV. From Paillous, Amat, Marco & Panabiere (1977) [97].	176
Figure 5-75: Effect of Protons Radiation on normal-hemispherical spectral reflectance, ρ'_{λ} , of PSZ 184 coating, on silicated primer, vs. wavelength, λ . Radiation intensity \cong 150 keV. From Paillous, Amat, Marco & Panabiere (1977) [97].	177
Figure 5-76: Effect of Electrons Radiation on normal-hemispherical spectral reflectance, ρ'_{λ} , of PSZ 184 coating, on silicated primer, vs. wavelength, λ . Radiation intensity \cong 40 keV. From Paillous, Amat, Marco & Panabiere (1977) [97].	178
Figure 5-77: Effect of Electrons Radiation on normal-hemispherical spectral reflectance, ρ'_{λ} , of PSZ 184 coating, on silicated primer, vs. wavelength, λ .	

CEN/CLC/TR 17603-31-06:2021 (E)

Radiation intensity \cong 80 keV. From Paillous, Amat, Marco & Panabiere (1977) [97].....	179
Figure 5-78: Effect of Electrons Radiation on normal-hemispherical spectral reflectance, ρ'_{λ} , of PSZ 184 coating, on silicated primer, vs. wavelength, λ . Radiation intensity \cong 210 keV. From Paillous, Amat, Marco & Panabiere (1977) [97].....	180
Figure 5-79: Effect of Combined Exposure, simulating up to three years in geosynchronous orbit, on normal-hemispherical spectral reflectance, ρ'_{λ} , of PSZ 184 coating, vs. wavelength, λ . From Paillous (1976) [96].....	181
Figure 5-80: Effect of O ₂ bleaching, after Combined Exposure, on normal-hemispherical spectral reflectance, ρ'_{λ} , of PSZ 184 coating, vs. wavelength, λ . Curves  and  are those shown in Figure 5-79. From Paillous (1976) [96].	182
Figure 5-81: Solar absorptance, α_s , of PCBZ coating vs. UV Radiation exposure time, t . From Guillaumon (1982) [48].....	189
Figure 5-82: Normal-hemispherical spectral reflectance, ρ'_{λ} , of PCBZ coating, sample A, vs. wavelength, λ . Effect of Ultra-Violet radiation.	192
Figure 5-83: Normal-hemispherical spectral reflectance, ρ'_{λ} , of PCBZ coating, sample C, vs. wavelength, λ . Effect of Ultra-Violet radiation.	193
Figure 5-84: Hemispherical total emittance, ε , of OCLI Type SI-100 Thermal Control Mirrors as a function of temperature, T . \circ :> From Breuch (1967) [22]. \square :> From Marshall & Breuch (1968) [80]. \triangle :> From Cunningham, Grammer & Smith (1969) [33]. Uncertainty limits are from Marshall & Breuch (1968) [80].....	201
Figure 5-85: Solar absorptance, α_s , of OCLI Type SI-100 Thermal Control Mirrors vs. incidence angle, β . The full lines in a correspond to the analytical geometries sketched in b. Circles are from solar reflectance measurements, and the dotted line is based on flight temperatures of the NEMS radiator. From Stultz (1976) [123].....	203
Figure 5-86: Change in solar absorptance, $\Delta\alpha_s$, of OCLI Type SI-100 Thermal Control Mirror vs. incidence angle, β , as deduced from data of COMSTAR D-1, D-2 and D-3 satellites. The envelopes contain all the data points. \circ :> Integrated sphere spectrophotometer measurements made on a single mirror. From Hyman (1981) [62].	204
Figure 5-87: Change in solar absorptance, $\Delta\alpha_s$, of OCLI Type SI-100 Thermal Control Mirrors vs. exposure time, t	207
Figure 5-88: Solar absorptance, α_s , of OSR Fused Silica Mirrors vs. orbital time, t , as deduced from data of NavStar 5.....	215
Figure 5-89: Solar absorptance, α_s , of OCLI Type SI-100 Thermal Control Mirrors vs. exposure time, t , as deduced from data of COMSTAR D-1, D-2 and D-3 satellites.  : Derived from> temperature telemetry.  : Corrected to> normal solar incidence.	220
Figure 5-90: Solar absorptance, α_s , of OCLI Type SI-100 Thermal Control Mirrors vs. exposure time, t , as deduced from data of SCATHA spacecraft.	223
Figure 5-91: Change in solar absorptance, $\Delta\alpha_s$, of OCLI Type SI-100 Thermal Control Mirrors vs. exposure time, t , as deduced from data of HELIOS-A and B spacecraft.	227

CEN/CLC/TR 17603-31-06:2021 (E)

Figure 5-92: Summary data on the change in solar absorptance, $\Delta\alpha_s$, of OCLI Type SI-100 Thermal Control Mirrors vs. exposure time, t .	229
Figure 5-93: Normal-hemispherical spectral reflectance, ρ'_λ , of OCLI Type SI-100 Thermal Control Mirrors vs. wavelength, λ . From Cunningham, Grammer & Smith (1969) [33].	230
Figure 5-94: Effect of Ultra-Violet radiation on normal-hemispherical spectral reflectance, ρ'_λ , of OCLI Type SI-100 Thermal Control Mirrors vs. wavelength, λ . From Cunningham, Grammer & Smith (1969) [33].	231
Figure 5-95: Effect of Combined Exposure, simulating up to seven years in geosynchronous orbit, on normal-hemispherical spectral reflectance, ρ'_λ , of OCLI Type SI-100 Thermal Control Mirrors vs. wavelength, λ . a Bonded sample. b Sample fastened bare. From Paillous (1975) [95].	240
Figure 5-96: Effect of Combined Exposure, simulating up to seven years in geosynchronous orbit, on normal-hemispherical spectral reflectance, ρ'_λ , of OCLI Type SI-100 Thermal Control Mirrors vs. wavelength, λ . Sample fastened bare. From Paillous (1975) [95].	241
Figure 5-97: Solar absorptance, α_s , of OCLI Type CC-SSM vs. incidence angle, β . Circles are calculated values. From Winkler & Stampfl (1975) [139].	255
Figure 5-98: Estimated change in solar absorptance, $\Delta\alpha_s$, of OCLI Type CC-SSM vs. exposure time, t . The tests simulate geosynchronous orbit exposure of the Orbital Test Satellite (OTS) equatorial faces.	256
Figure 5-99: Change in solar absorptance, $\Delta\alpha_s$, of OCLI Type CC-SSM vs. exposure time, t . The insert shows the changes in α_s which suddenly results when ultra-violet exposure, at 16 Suns, begins.	258
Figure 5-100: Solar absorptance, α_s , of OCLI Type CC-SSM vs. exposure time, t as deduced from data of SCATHA spacecraft.	260
Figure 5-101: Change in solar absorptance, $\Delta\alpha_s$, of OCLI Type CC-SSM vs. exposure time, t as deduced from data of HELIOS-A and B spacecraft. Line of circles: First HELIOS-A orbit. Simplified model of data analysis.	261
Figure 5-102: Summary on the change in solar absorptance, $\Delta\alpha_s$, of OCLI Type CC-SSM vs. exposure time, t . The estimated values of the initial solar absorptance, α_{so} , are shown near each curve.	262
Figure 5-103: Effect of Combined Exposure, simulating up to three years in geosynchronous orbit, on normal-hemispherical spectral reflectance, ρ'_λ , of OCLI Type CC-SSMs vs. wavelength, λ . From Paillous (1976) [96].	263
Figure 5-104: a. Electrical resistance, R , of six CC-SSM samples as a function of temperature, T . b shows the two alternative configurations of the electrical contacts set for performing the measurements. From Joslin & Kan (1975) [67].	264
Figure 5-105: a. Sheet electrical resistance, R , of three OCLI Type CC-SSMs vs. time in simulated geosynchronous orbit, t . b. Configuration of the electrical contacts and position of the mirrors on the sample holder for irradiation and measurements. From Paillous (1976) [96].	269
Figure 5-106: Normal-hemispherical spectral reflectance, ρ'_λ , of Fuller 172A1, vs. wavelength, λ . From Touloukian, DeWitt & Hernicz (1972) [126].	277

CEN/CLC/TR 17603-31-06:2021 (E)

Figure 5-107: Normal-hemispherical spectral reflectance, ρ'_{λ} , of Fuller 172A1, exposed to gamma radiation, vs. wavelength, λ . From Touloukian, DeWitt & Hernicz (1972) [126].	278
Figure 5-108: Normal-hemispherical spectral reflectance, ρ'_{λ} , of Kemacryl M49BC12, vs. wavelength, λ . From Touloukian, DeWitt & Hernicz (1972) [126].	281
Figure 5-109: Normal-hemispherical spectral reflectance, ρ'_{λ} , of Kemacryl M49BC12, exposed to gamma radiation, vs. wavelength, λ . Points of white circles are those represented in Figure 5-108. From Touloukian, DeWitt & Hernicz (1972) [126].	282
Figure 6-1: Peel force, probe tack and rolling ball tack, F , as functions of resin concentration, c , for a rubber adhesive on a polyethylene terephthalate (polyester) film.	284
Figure 6-2: Peel adhesion, F/w , measured at 393 K as a function of curing temperature, T . Rubber based adhesive. From Toyama & Ito (1974) [127].	285
Figure 6-3: Space degradation of second surface mirrors based on $1,27 \times 10^{-4}$ m thick FEP Teflon. All data are from Triolo (1973) [128] except those corresponding to IMP-I which are from Hoffman (1973) [61].	303
Figure 6-4: Sketch of a blistering tape. From Brown & Merschel (1970) [23].	304
Figure 6-5: Solar absorptance, α_s , vs. total hemispherical emittance, ε , of several thermal control tapes.	307

Tables

Table 5-1: Ultra-Violet Radiation Effects on Spectral Absorptance of Thermatrol 2A-100.	27
Table 5-2: Solar Absorptance of Zinc Oxide-Potassium Silicate Paint	34
Table 5-3: Ultra-Violet Radiation Effects on Spectral Absorptance of Zinc Oxide-Potassium Silicate Paint.	36
Table 5-4: Ultra-Violet Radiation Effects on Solar Absorptance of Zinc Oxide-Potassium Silicate Paint	43
Table 5-5: Literature Search for Thermal radiation Properties of ZOT Coatin	55
Table 5-6: Solar Absorptance of Zinc Orthotitanate-Potassium Silicate Coatings ^a	61
Table 5-7: Ultra-Violet Radiation Effects on Solar Absorptance of Zinc Orthotitanate-Potassium Silicate Coatings ^a	63
Table 5-8: Hemispherical Total Emittance of S-13 and S-13 G Coating	85
Table 5-9: Ultra-Violet Radiation Effects on Hemispherical Total Emittance of S-13 and S-13 G Coating	86
Table 5-10: Normal Total Emittance of S-13 G and S-13 G-LO Coatings	88
Table 5-11: Ultra-violet radiation effects on spectral absorptance of S-13 coating (samples 27 & 28)	90
Table 5-12: Ultra-Violet Radiation Effects on Solar Absorptance of S-13 and S-13 G Coatings	93
Table 5-13: Combined Exposure Effects on Solar Absorptance of S-13 G/LO Coating	102
Table 5-14: Outgassing Characteristics of PSG 120 Coating	138

CEN/CLC/TR 17603-31-06:2021 (E)

Table 5-15: Protons Radiation Effects Solar Absorptance of PSG 120 Coating	144
Table 5-16: Electrons Radiation Effects on Solar Absorptance of PSG 120 Coating	145
Table 5-17: Combined Exposure Effects on Solar Absorptance of PSG120 Coating	146
Table 5-18: Application of the Degradation Model to PSG 120 Coating	156
Table 5-19: Test Conditions Simulating up to Three Years in Geosynchronous Orbit	159
Table 5-20: Hemispherical Total Emittance, ε , and Solar Absorptance, α_s , of PSZ 184	165
Table 5-21: Protons Radiation Effects on Solar Absorptance of PSZ 184 Coating	169
Table 5-22: Electrons Radiation Effects on Solar Absorptance of PSZ 184 Coating	170
Table 5-23: Combined Exposure Effects on Solar Absorptance of PSZ 184 Coating	171
Table 5-24: Outgassing Characteristics of PCB Z Coating	187
Table 5-25: Ultra-Violet Radiation Effects on Solar Absorptance of PCBZ Coating	189
Table 5-26: Charging Tests with PCBZ Coating	194
Table 5-27: Candidate Adhesives for OSR Fused Silica Application	198
Table 5-28: Ultra-Violet Radiation Effects on Spectral Absorptance of OCLI Type SI-100 Thermal Control Mirrors	205
Table 5-29: Test Conditions Simulating up to Seven Years in Geosynchronous Orbit	232
Table 5-30: Combined Exposure Effects of Reflectance of OCLI Type SI-100. Thermal Control Mirrors.	234
Table 5-31: Charging-Arcing Tests with OCLI Type SI-100 Thermal Control Mirrors	243
Table 5-32: Normal Total Emittance, ε' , and Solar Absorptance, α_s , of Several OCLI Type Thermal Control Mirrors	255
Table 5-33: Effects of Simulated Geosynchronous Orbit Exposure on Solar Absorptance of OCLI Type CC-SSM	257
Table 5-34: Protons (Electrons) Only Exposure Effects on Sheet Resistance of OCLISolar Cell Cover Slides	265
Table 5-35: Protons (Electrons) Only Exposure Effects on Resistance of Conductive Coated Fused Silica	266
Table 5-36: Change in the Specific Electrical Cross Resistance, ρ_c , of OCLI Type CC-SSMs by Outgassing Silastic Materials	268
Table 5-37: Charging Tests with OCLI Type CC-SSMs	271
Table 5-38: Hemispherical Total Emittance and Solar Absorptance of Leafing Aluminium-Silicone	275
Table 5-39: Hemispherical Total Emittance and Solar Absorptance of Carbon Black-Acrylic Resin	280
Table 6-1: Thermosetting Cure Cycles and Useful Temperature Range of Several MYSTIK Adhesive Tapes.	286
Table 6-2: Properties of Double-Faced Adhesive Tapes ^a	287
Table 6-3: Properties of Unsupported Adhesive Tapes ^a	296
Table 6-4: Several Solvents of the Adhesives	299
Table 6-5: Rubbing Degradation of the Optical Properties of Aluminized Films	299

CEN/CLC/TR 17603-31-06:2021 (E)

Table 6-6: Thermal radiation Properties of Second Surface Silver-Teflon ($1,27 \times 10^{-4}$ m thick)	301
Table 6-7: Exposure Conditions of Silver-Teflon on IMP-I Spacecraft.....	304
Table 6-8: Blistering Temperatures of Tapes Applied to an Aluminium Substrate ^a	305
Table 6-9: Properties of First Surface Metallized Tapes ^a	308
Table 6-10: Properties of Second Surface Metallized Tapes ^a	314
Table 6-11: Properties of Clear Tapes ^a	324
Table 6-12: Mass-Area Ratio of Several Foils and Tapes.....	328
Table 6-13: Characteristics of Low-Outgassing Tapes ^a	329

European Foreword

This document (CEN/CLC/TR 17603-31-06:2021) has been prepared by Technical Committee CEN/CLC/JTC 5 “Space”, the secretariat of which is held by DIN.

It is highlighted that this technical report does not contain any requirement but only collection of data or descriptions and guidelines about how to organize and perform the work in support of EN 16603-31.

This Technical report (TR 17603-31-06:2021) originates from ECSS-E-HB-31-01 Part 6A.

Attention is drawn to the possibility that some of the elements of this document may be the subject of patent rights. CEN [and/or CENELEC] shall not be held responsible for identifying any or all such patent rights.

This document has been prepared under a mandate given to CEN by the European Commission and the European Free Trade Association.

This document has been developed to cover specifically space systems and has therefore precedence over any TR covering the same scope but with a wider domain of applicability (e.g.: aerospace).

1

Scope

This Part 6 of the spacecraft thermal control and design data handbooks, provides information on coatings on spacecrafts for the purposes of thermal and thermo-optical regulation.

Properties of pigmented and contact coatings, are described and are classified according to their thermal radiation characteristics.

Also included in this Part are the properties and characteristics of foils and tapes with particular emphasis on their adhesive characteristics; these are not classified according to their thermal radiation properties.

The Thermal design handbook is published in 16 Parts

TR 17603-31-01	Thermal design handbook – Part 1: View factors
TR 17603-31-02	Thermal design handbook – Part 2: Holes, Grooves and Cavities
TR 17603-31-03	Thermal design handbook – Part 3: Spacecraft Surface Temperature
TR 17603-31-04	Thermal design handbook – Part 4: Conductive Heat Transfer
TR 17603-31-05	Thermal design handbook – Part 5: Structural Materials: Metallic and Composite
TR 17603-31-06	Thermal design handbook – Part 6: Thermal Control Surfaces
TR 17603-31-07	Thermal design handbook – Part 7: Insulations
TR 17603-31-08	Thermal design handbook – Part 8: Heat Pipes
TR 17603-31-09	Thermal design handbook – Part 9: Radiators
TR 17603-31-10	Thermal design handbook – Part 10: Phase – Change Capacitors
TR 17603-31-11	Thermal design handbook – Part 11: Electrical Heating
TR 17603-31-12	Thermal design handbook – Part 12: Louvers
TR 17603-31-13	Thermal design handbook – Part 13: Fluid Loops
TR 17603-31-14	Thermal design handbook – Part 14: Cryogenic Cooling
TR 17603-31-15	Thermal design handbook – Part 15: Existing Satellites
TR 17603-31-16	Thermal design handbook – Part 16: Thermal Protection System

2 References

EN Reference	Reference in text	Title
EN 16601-00-01	ECSS-S-ST-00-01	ECSS System - Glossary of terms
TR 17603-31-09	ECSS-E-HB-31-01 Part 9	Thermal design handbook – Part 9: Radiators
TR 17603-31-12	ECSS-E-HB-31-01 Part 12	Thermal design handbook – Part 12: Louvers
TR 17603-31-15	ECSS-E-HB-31-01 Part 15	Thermal design handbook – Part 15: Existing Satellites

All other references made to publications in this Part are listed, alphabetically, in the **Bibliography**.

koniec náhľadu – text ďalej pokračuje v platenej verzii STN